COBEM 2023 27TH INTERNATIONAL CONGRESS OF MECHANICAL ENGENEERING

ABCM Brazilian Society of Mechanical Sciences and Engineering
27th ABCM International Congress of Mechanical Engineering
December 04-08, 2023, Florianópolis-SC, Brazil

COB-2023-1754
EXPERIMENTAL INVESTIGATION OF HVOF AND POLYMERIC COATINGS FOR TURBINE BLADE PROTECTION

Fabio Antonio Xavier
Carlos Enrique Niño Bohórquez
Rodrigo Bastos Fernandes
Fernando Moreira Bordin
Erick Cardoso Costa
Miguel Carvalho Barcelos
Beatriz Cardoso Santos
Universidade Federal de Santa Catarina, Departamento de Engenharia Mecânica, Centro Tecnológico, Campus Reitor João David Ferreira Lima, Trindade, Florianópolis, Brazil
f.xavier@ufsc.br
carlos.nino@ufsc.br
fernandes.r@ufsc.br
f.m.bordin@posgrad.ufsc.br
erick.cardoso.costa@posgrad.ufsc.br
miguel.barcelos@posgrad.ufsc.br
beatrizcardoso1003@gmail.com

Leandro Luiz de Oliveira e Silva
Waldson Melo Bezerra
Jirau Energia, Distrito de Jaci Paraná – Porto Velho (RO)
leandro.oliveira@jirauenergia.com.br
waldson.bezerra@jirauenergia.com.br

Abstract. *Hydroelectric power plant maintenance is a very costly and time-consuming activity, especially when the main cause of turbine blade wear is the severe abrasion caused by a large amount of abrasive sediment. Abrasion-resistant coatings are used to mitigate this problem. However, the limited time for turbine maintenance, associated with many turbines, confined space, and health and safety concerns, limits the methods of coating application. This study presents a comparison between two popular coating application methods: thermal spray by high-velocity oxygen fuel (HVOF) and polymeric application by trowel/brush. The objective is to evaluate the performance of commercial coating materials, which are largely used for abrasion and cavitation wear of turbine blades, under a dry sand/rubber wheel abrasion apparatus, following ASTM G65. The coating materials were evaluated in terms of wear resistance and behavior, versus the estimated application time, to compare the time-effectiveness of commercial coatings. The coatings were applied onto AISI 316L stainless steel samples, with a minimum thickness of 300 µm (HVOF coatings) and 600 µm (polymeric coatings). The coating materials were characterized in terms of overall thickness, hardness by macro and microindentation, and subsurface morphology: phases and chemical elements. The experiments were performed in a dry sand/rubber wheel abrasometer, using Procedure D with a maximum number of revolutions equal to 6000, a loading of 45 N applied by a cantilever loading system. A load cell, supervised by a microcontroller, was fixed to the specimen fixture, to calibrate the static load onto the workpiece, and to closely follow the normal force behavior during the experiments. The results were evaluated in terms of wear rate behavior (adjusted volume loss divided by time) of each measuring interval, followed by the cavity profile and normal force signals, along with the estimated application time. There is a significant advantage for the HVOF coated specimen in terms of wear resistance. However, the health, safety, and lower necessary time to apply polymeric coating may justify the increasing interest in this type of coating material, ultimately leaving the decision of the most time-effective coating material to the end-user.*

Keywords: *Hydroeletric power plant, abrasion resistant coatings, ASTM G65, wear behavior, performance evaluation.*

1. INTRODUCTION

Hydropower is a reliable renewable source of energy, contributing with an overall 17% of the total energy generation around the globe. However, hydropower plants suffer with silt erosion, impeding its quality, impairing the durability and reliability of the turbine blades (Kumar e Saini, 2021). Surface damages caused by fatigue, corrosion, and wear (abrasive and cavitation erosion) are among the main causes that lead to failure of hydropower plant components (Ciubotariu *et al.*, 2016). The maintenance of hydroelectric turbine blades is a periodic and necessary phase, which aims to maintain the

performance of electric energy production, as well as extending the service life of the energy generation subsystem. Contextually, the Madeira River is one of the most abrasive rivers, with high concentration of abrasive silts, which in turn requires materials that withstand the intense abrasive damage to avoid frequent and extensive repairs (Lima *et al.*, 2014).

A variety of techniques, such as electro-spark deposition, arc welding, laser surface melting, thermal spray, cold spray has been explored to strengthen/coat the cavitation and abrasion resistance of hydropower components (Jiang *et al.*, 2020). However, the increasing concern for the sustainability of the process chain leads not only the need for sustainable energy generation (Hauer *et al.*, 2018), but to an effective and sustainable technology applied for turbine blade protection.

Thermal spray process, one of the most usual application processes for turbine blade protection, emits ultrafine particles that, associated with powder atomization and difficulty to collect, leads to a hazardous work environment (Darut *et al.*, 2021). This leads to an increased interest on applying polymeric epoxy resin-based materials as a protective barrier for abrasion and cavitation wear, due to its relatively clean application environment and higher material deposition rates.

Polymers and polymers blends can be reinforced with fibers or particles to form a polymer composite, enabling an increase in stiffness, toughness and strength, which makes polymer-based materials promising due to the ability to control and optimize wear behavior in tribological contacts for a more sustainable and green hydropower industry (Somberg *et al.*, 2021).

Therefore, this study aims to compare the abrasive wear resistance of a commercial polymer (epoxy resin) coating in comparison to commercial thermal spray (tungsten carbide obtained by high velocity oxygen fuel – HVOF) coating.

2. MATERIALS AND METHODS

2.1 General overview

The experiments were performed according to the ASTM G65-16 standards, which describes a procedure to evaluate the abrasion resistance of materials by using a steel disc with a thick layer of rubber to create sliding motion. A workpiece is pushed against the rubber wheel with a selected normal force. Dry sand is introduced in the interface between the rubber wheel and the workpiece by a nozzle, acting as abrasive media. This procedure creates an accelerated abrasion wear mechanism.

The standard specifies five possible procedures, that range from severe to mild conditions, in which the normal force and number of wheel revolutions is altered. Screening tests were performed to evaluate the conditions that suited both coating materials: tungsten carbide coatings have a higher abrasion resistance than polymer coatings and thus, procedure D was selected (normal load of 45 N and a number of 6000 wheel revolutions). The number of revolutions was used to segment the experiment in 6 intervals. The end of life of a coated sample selected was either reaching the threshold of revolutions or removal of the coating material.

As per methodology, prior to the experiments and after each number of revolutions interval, the sample is cleaned in ultrasonic bath, dried, and weighted using a semi-analytic balance. The weight is registered and used to calculate the adjusted volume loss (AVL) and the wear rate (WR), according to the Eq. (1) and Eq. (2), respectively:

$$AVL = v_{loss} \times \frac{228.6\ mm}{d_{wheel,f}}, \tag{1}$$

$$WR = AVL/t, \tag{2}$$

where, v_{loss}, $d_{wheel,f}$, and t are the volume loss (converted from mass variation using the specific mass) in mm^3, rubber wheel diameter after use in mm, and time in minutes, respectively. A total of 5 samples per coating material were experimented on.

2.2 Workpiece

The samples were manufactured in AISI 316L stainless steel, machined in a rectangular shape of dimensions: 55 mm x 22 mm x 12.7 mm. The surface that received the coating material was sand blasted to reach an average surface roughness (Ra) of 6 µm, maximum surface roughness (Rz) of 30 µm. The samples were coated with two distinct commercial coating materials, obtained by HVOF thermal spray process (tungsten carbide matrix) and by manual application by trowel (polymeric matrix), dubbed: WC and POL, respectively. The sample manufacturing was performed by the coating supplier, as means to compare the service provided. Table 1 describes the coating materials and specifications.

Table 1. Coating materials specifications.

Nomenclature	Coating process	Specification	Nominal thickness	Density
WC	HVOF	WCCoCr 86 10 4	300 ± 25 µm	13.97 g/cm^3
POL	Manual	Epoxy resin	600 ± 50 µm	2.44 g/cm^3

The surface of the samples was ground to obtain a flat and smooth surface, with a maximum surface roughness (Ra) of 0.8 µm. Samples prior to the tests were evaluated in terms of overall structure by scanning electron microscopy, as well as composition by energy dispersive spectroscopy and Fourier Transform Infrared spectroscopy FTIR (polymeric coating only). Coating thickness was estimated by image analysis (segmentation, classification and binarization) using an open-source software, ImageJ. Figure 1 illustrates the results of the WC coating characterization.

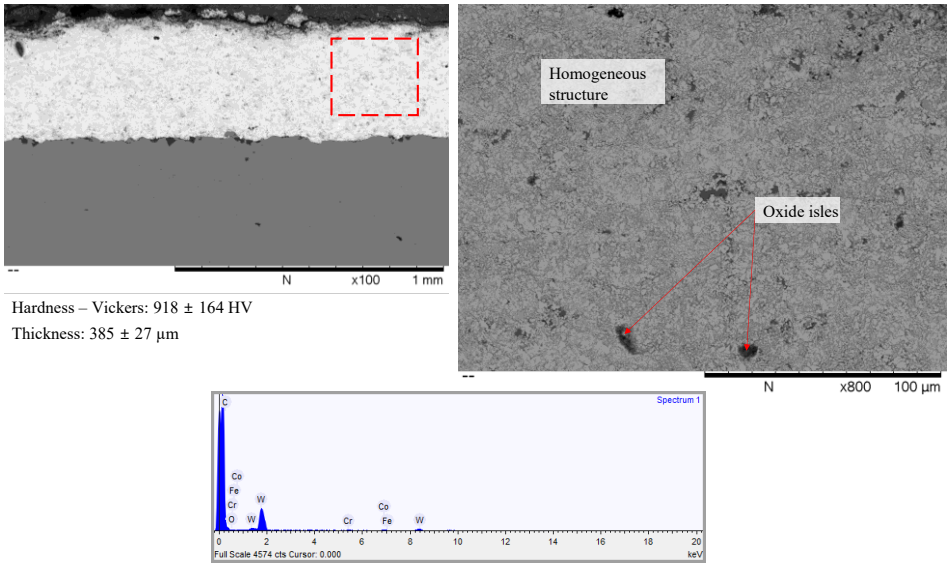

Figure 1. Scanning electron microscopy, EDS spectrum and mechanical properties of the WC-coated samples.

The tungsten carbide coatings present homogeneous structure, where hardness and consequently wear resistance derives from the ceramic and metallic materials composition. There are isolated oxide isles, resulting from contamination of the powder used during the coating process. The EDS spectrum, although qualitative, reinforces the oxide presence hypothesis. Other elements like W, C, Co and Fe were also detected. Analysis of the structure and composition of the polymeric coating is shown in Figure 2.

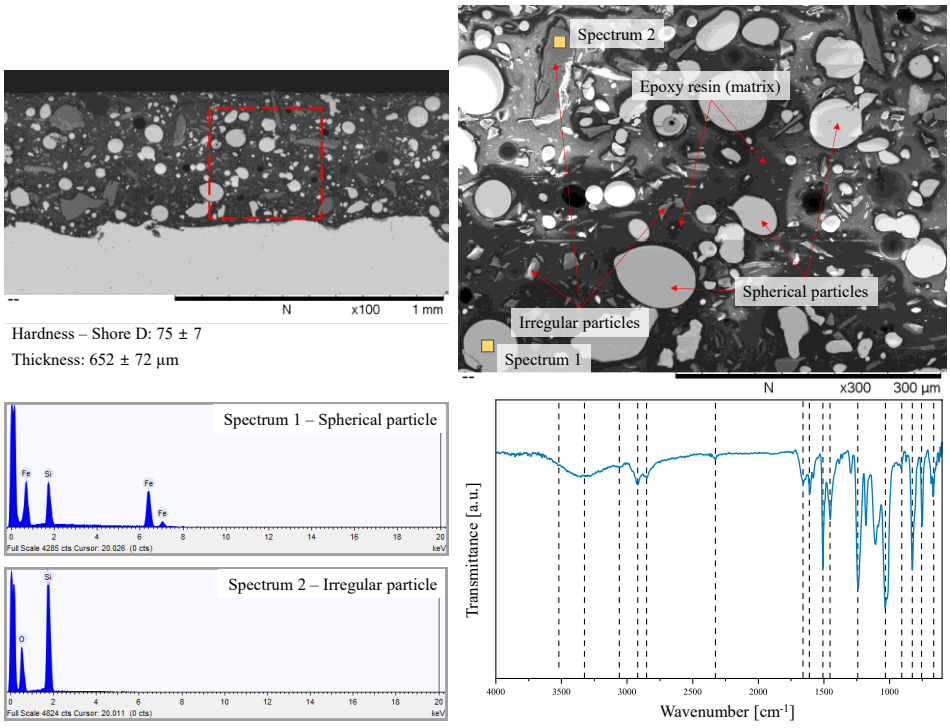

Figure 2. Scanning electron microscopy, EDS and FTIR spectrum and mechanical properties of the polymeric-coated samples.

The polymeric coating, in contrast, showcases a heterogeneous structure, with a defined matrix and hard particles dispersed. The particles are presented in regular (spherical shapes) and irregular geometry and sizes. The measured Shore D hardness is representative of the epoxy resin matrix, since measuring hardness for particles embedded in a soft matrix is not trivial. The EDS spectrum revealed presence of iron and silicon in the spherical particles, which may be associated with Ferro Silicon phase, used to increase hardness and grant abrasive resistance. Complementary, the irregular particles presented traces of silicon and oxygen, likely related to Silicon Dioxide (SiO_2), a hard and brittle phase which also inherently increases abrasion resistance.

FTIR spectrum identified absorption bands characteristics of epoxy resin with benzenic structure, such as: deformation of the hydroxyl (OH) group 3325 cm^{-1}, in the range 2920-2850 (CH deformation), 1612 (C=C), 1242 (ether group), 1032 (hydroxyl group, as well as C-N), 907 (epoxy ring), 900-675 (C-H aromatic).

An average thickness of 652 ± 72 µm was measured, which denotes an uneven surface. Characterizations of the surface pre-grinding process, using a Taylor Hobson FTS i-120 profilometer, expressed a maximum waviness deviation (Wz) of 289 ± 160 µm, which also corroborates for the unevenness of the coated surface. The coating WC presented an average thickness of 385 ± 27 µm, and a maximum waviness deviation of 12 ± 4 µm, denoting a more even surface pre-surface preparation.

2.3 Experimental setup

The experiments were carried out according to the specifications in section 2.1. As constant parameters, and in accordance with the ASTM G65, it was employed a rubber wheel rotation n_{wheel} of 205 min^{-1}, mass flow of 380 g/min, normal load of 45 N (Procedure D). Silicon dioxide (SiO_2), mesh 50, was used as abrasive, supplied following the normative NBR 7214.

In order to verify the normal force on the workpiece, a strain gauge-based load cell was adapted to the workpiece holder, used to perform the weight adjustment at the end of the cantilever arm. The load cell was connected to a microcontroller, which also allowed acquisition of the normal force and rubber wheel revolutions during the experiments, with a sample rate (f_s) of 10 Hz. Figure 3 illustrates an overview of the machine/abrasion apparatus.

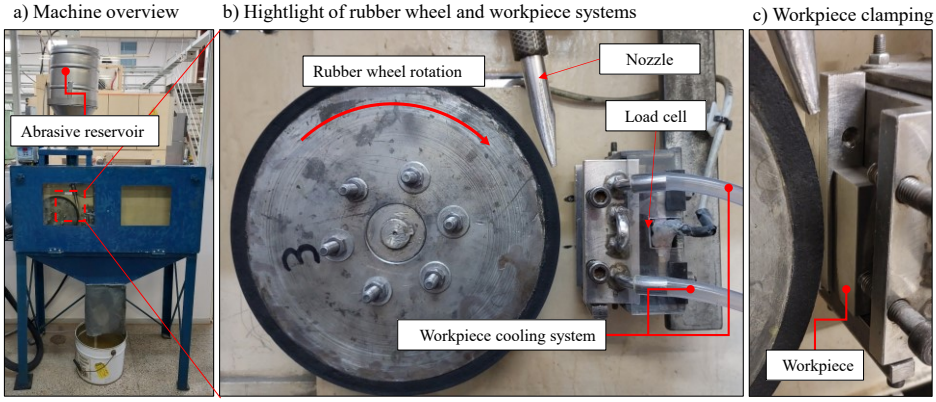

Figure 3. Machine structure: (a) external overview, (b) inner details and (c) close view of the workpiece holder.

2.4 Analysis

Sample adjusted volume loss was compiled in terms of wear rate at each intermediate interval. The cavity wear was measured following the longitudinal and transversal profile using a Taylor Hobson FTS i-120 profilometer, and the resulting surface texture of the cavity was obtained using a scanning electron microscope, Hitachi, TM3030. The normal force signals were registered and plotted against the wear curves highlighting the behavior, as to identify any possible trends.

3. RESULTS AND DISCUSSIONS

The worn material was monitored by weighting the samples throughout the experiments, complemented by time monitoring. The wear rate (WR), therefore, was computed by the input value of the two monitored entries. Figure 4 illustrates the wear behavior for both coated samples.

There is a distinctive difference between the two coated samples. The average magnitude of the wear rate is several orders of magnitude higher for the polymeric (140 mm^3/min) resin when compared to the tungsten carbide (0.05 mm^3/min). Although the wear behavior of the tungsten carbide samples (Fig. 4a) illustrates a large dispersion, by isolating each sample, it is possible to describe a pattern: higher wear at the start of the experiment, decreasing as time increased.

This pattern is better observed for the polymeric coating (Fig. 4b), where there is a sharp increase in wear rate at the start of the cycle, that decreases and reaches a threshold. This new platform is marked by a constant wear rate, before the abrupt interruption of the experiment, highlighted by the total removal of the coating at the center of the sample.

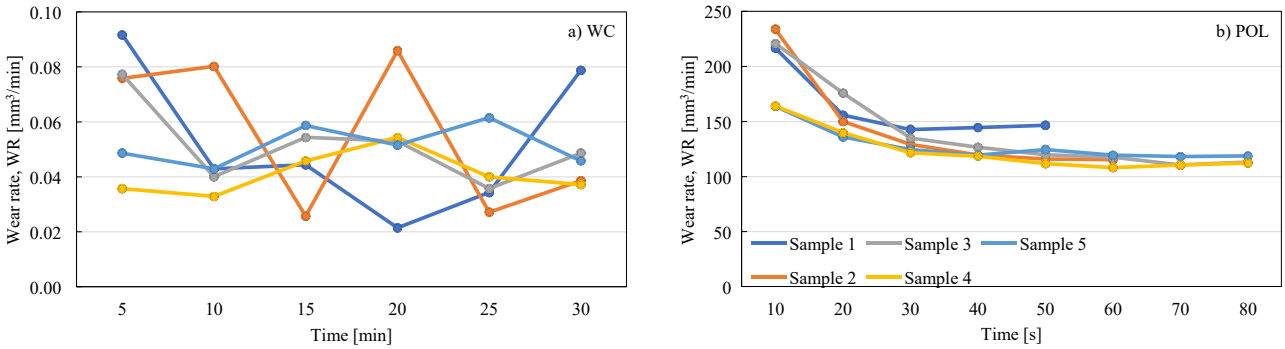

Figure 4. Abrasive wear behavior of the samples coated with tungsten carbide (a) and polymeric resin (b).

This behavior is the result of the initial contact, denoted by a flat surface against a curvy surface and since a constant static load is applied to the workpiece holder, the initial contact pressure is higher. As the sample wears, the contact area increases, leading to a reduction in the contact pressure. This is well stablished for the POL samples, since the WC sample did not wear down enough to present an extreme alteration on the sample profile, shown in Fig. 5.

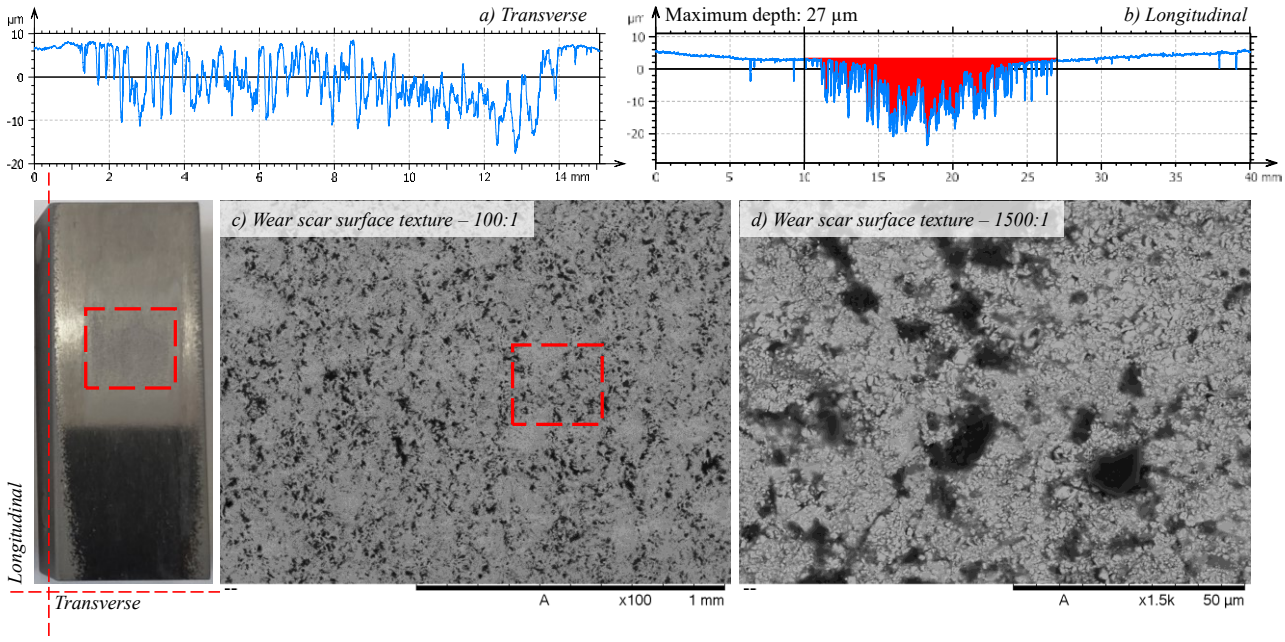

Figure 5. Detail of the abrasive wear cavity: transverse (a) and longitudinal (b) profiles; surface texture with magnifications of 100x (c) and 1500x (d).

The wear cavity/scar, highlighted within the leftmost rectangle, is barely visible on the sample's photography, presenting a maximum depth of the wear cavity of 28 µm. This behavior is due to the high hardness and resistance to abrasive wear. Since the longitudinal profile (Fig. 5a) of the cavity shows a rough surface, with several peaks and valleys, such results indicate a mechanism of brittle material removal. The transverse profile (Fig. 5b) of the center of the cavity has a similar pattern and, thus, does not indicate a discernable direction of cutting, which supports the brittle mechanism hypothesis. The surface texture (Fig. 5c and detailed in Fig. 5d) illustrates a random surface, with no discernible deformation/cutting pattern. Kumar *et al.* (2023) studies on the mechanism of slurry erosion (SE) of coatings also transcribe a list of authors that found similar wear behavior for the WC-CoCr coatings, associating the mechanism with an acute incidence angle that causes crack initiation and propagation, rather than plastic deformation due to the high hardness and brittleness of the material.

For the POL samples, the longitudinal profile (Fig. 6b) exhibits a negative replica of the rubber wheel curvature, indicating a severe abrasive wear. Even with a reinforced structure of the polymeric material, embedded with spherical

and irregular ceramic phases, the low abrasive resistance of the polymeric matrix did not withstand the severity of the abrasion experiments. The transverse profile (Fig. 6a) did not illustrate a specific feature. The observation of the wear cavity on the photography hints of a cutting mechanism rather than brittle fracture.

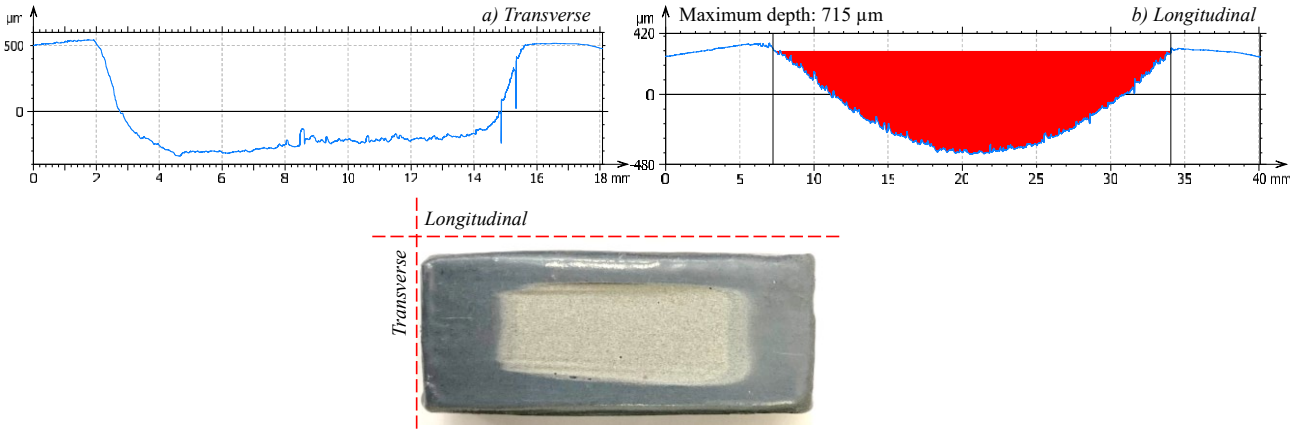

Figure 6. Detail of the abrasive wear cavity: transverse (a) and longitudinal (b) profiles.

When analyzing the normal force (Fn) across the experiments, it is possible to notice two distinct zones: a first contact zone (Fig. 7c), where the normal force exhibits a sharp increase during the initial contact of the rubber wheel against the workpiece, caused by the adjustment of the rubber wheel geometry to the workpiece surface, decreasing slowly; and a stabilization zone (Fig. 7d), where normal forces stabilize around an average value. As the time increases, the necessary time to reach the stabilization zone decreases.

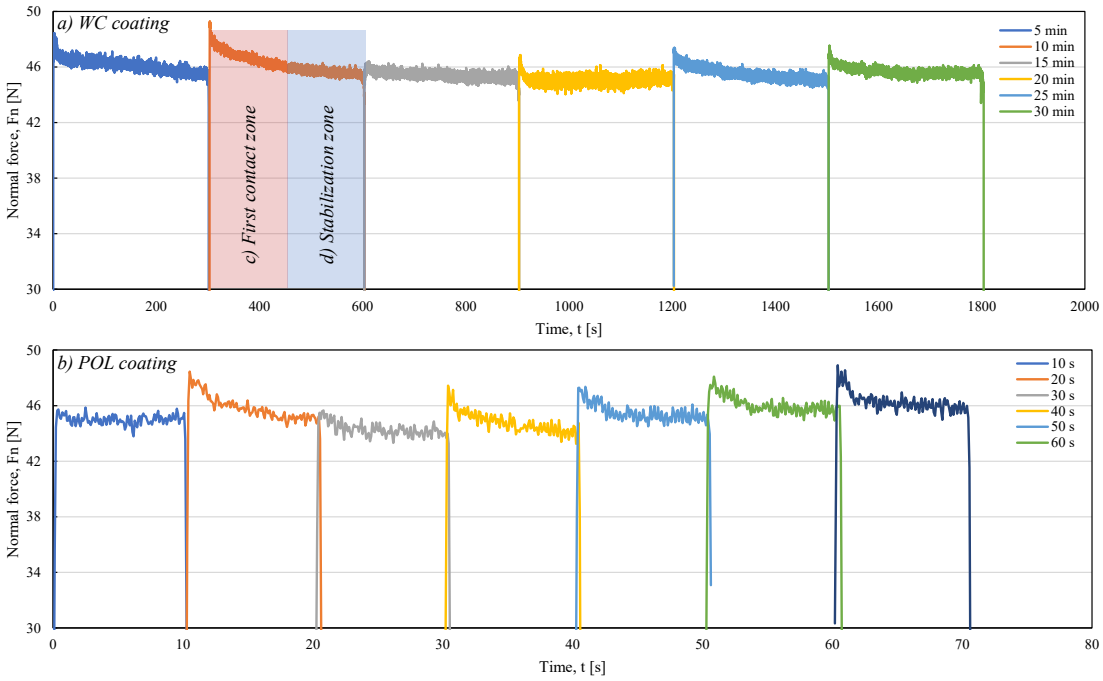

Figure 7. Normal force behavior during the experiments, detailing: (a) WC coating, (b) POL coating, (c) first contact zone and (d) stabilization zone.

A glance at the force behavior for both coatings (Fig.7 a, b) does not introduce a discernable trend. The force signals, although valuable to indicate the state of the cavity profile, does not present any significant difference between the analyzed coating materials and, therefore, mechanism of material removal. The first 3 segments of the POL sample experiment are situated in the region of “adjustment” of the workpiece geometry (sample 3, Fig. 4b), where largest variation of first contact and stabilization zones can be observed; the following normal force plots shows a similar behavior, in agreement with the observed wear.

Evidence, therefore, points out to an exceedingly higher abrasive wear resistance for the WC-CoCr coating more than the epoxy resin coating; but when considering the drawbacks in terms of sustainability presented by the HVOF process, it is necessary to further evaluate an additional aspect: coating time.

A quick analysis of the time necessary to apply the coating (Tab. 2) to an area of 60 m^2 (area of 4 turbine blades) illustrates that: although the polymeric coating possesses a lower abrasion resistance, the necessary time and easiness to apply the coating material may justify its application as a sacrifice material, instead of a higher resistance material such as an HVOF WC-CoCr coating.

Table 2. Average time for the coating process.

Nomenclature	Coating process	Thickness	Coating rate	Deposited mass	Deposition Efficiency	Time (coating + curing)
WC	HVOF	300 µm	0.067 kg/min	85 kg	100 %	47 h
POL	Manual	600 µm	0.0375 kg/min	420 kg	60 %	91 h

4. CONCLUSIONS

An overview of the results shows a large advantage of the WC-CoCr coating by HVOF in terms of abrasion resistance. The average abrasion resistance of the WC coating was 0.05 mm^3/min, several magnitude superiors to 140 mm^3/min, observed for the POL coating.

The WC coating is composed of a homogeneous structure, while the POL coating presents an epoxy resin with several irregular and spherical particles dispersed in a heterogeneous structure, undoubtedly, to increased resistance. However, in face of the severe experiments' conditions, the POL underperformed.

The main wear mechanism observed for the WC coating was brittle fracture, whereas for the POL coating was abrasion sliding leading to cutting.

5. ACKNOWLEDGEMENTS

This work was funded by Jirau Energia S.A. under grant number PD-06631-0013/2020. Project regulated by ANEEL and developed in the scope of R&D of Jirau Energia S.A.

6. REFERENCES

ASTM G65-16, 2016, Standard Test Method for Measuring Abrasion Using the Dry Sand/Rubber Wheel Apparatus, 14 p.

Ciubotariu, C.R., Frunzaverde, D., Marginean, G., Serban, V.A., and Birdeanu, A. V., 2016, Optimization of the laser remelting process for the HVOF-sprayed Stellite 6 wear resistant coatings, Optics & Laser Technology, Vol. 77, pp. 98-103.

Darut, G., Dieu, S., Schnuriger, B., Vignes, A., Morgeneyer, M., Lezzier, F., Devestel, F., Vion, A., Berguery, C., Roquete, J., and Bihan, O. L. B., 2021, State of the art of particle emissions in thermal spraying and other high energy processes based on metal powders, Journal of Cleaner Production, Vol. 303, pp. 126952.

Hauer, C., Wagner, B., Aigner, J., Holzapfel, P., Flödl, P., Lidermann, M., Tritthart, M., Sindelar, C., Pulg, U., Klösch, M., Haimann, M., Donnum, B. O., Stickler, M., and Habersack, H., 2018, State of the art, shortcomings and future challenges for a sustainable sediment management in hydropower: A review, Renewable and Sustainable Energy Reviews, Vol. 98, pp. 40-55.

Jiang, X., Overman, N., Smith, C., and Ross, K., 2020, Microstructure, hardness and cavitation erosion resistant of different cold spray coatings on stainless steel 316 for hydropower applications, Materials Today Communications, Vol. 25, pp. 101305.

Kumar, K. and Saini, R.P., 2021, Application of machine learning for hydropower plant silt data analysis, Materials Today: Proceedings, Vol. 46, pp. 5575-5579.

Kumar, M., Yadav, Y. K., Singh, A. K., and Siddhartha, 2023, Mechanisms of slurry erosion in coatings of hydro-turbines, Materials Today: Proceedings, Vol. n.a.

Lima, C.R.C., Libardi, R., Camargo, F., Fals, H.C., and Ferraresi, V.A., 2014, Assessment of Abrasive Wear of Nanostructured WC-Co and Fe-Based Coatings Applied by HP-HVOF, Flame, and Wire Arc Spray, Journal of Thermal Spray Technology, Vol. 23, pp. 1097-1104.

Somberg, J., Saravanan, P., Vadivel, H.S., Berglund, K., Shi, Y., Ukonsaari, J. and Emami, N., 2021. Tribological characterization of polymer composites for hydropower bearings: Experimentally developed versus commercial materials, Tribology International, Vol. 162, pp. 107101.

7. RESPONSIBILITY NOTICE

The authors are the only responsible for the printed material included in this paper.